中国激光

宽调谐高脉冲能量的短波红外光学参量振荡器

刘鹏翔[1,2,3,4]，李伟[1,2,3]，祁峰[2,3*]，牛春草[1,2,3]，李惟帆[2,3]，付俏俏[2,3,4]，郭丽媛[2,3]，李忠洋[5]

[1]沈阳化工大学信息工程学院，辽宁 沈阳 110142；

[2]中国科学院沈阳自动化研究所，辽宁 沈阳 110169；

[3]辽宁省太赫兹成像与感知重点实验室，辽宁 沈阳 110169；

[4]中国科学院大学，北京 100049；

[5]华北水利水电大学电力学院，河南 郑州 450045

摘要 利用Nd:YAG激光泵浦磷酸氧钛钾晶体，实现了波长为2.05～2.97 μm的相干光输出，其覆盖了近红外与中红外过渡波段(也称"短波红外波段")。采用了与以往报道不同的相位匹配调谐区域，在较小的晶体转角下，获得了较宽的调谐范围。比较了单程与双程泵浦的两种光学参量振荡器结构，验证了双程泵浦的优越性。双程泵浦的光学参量振荡器的最高输出脉冲能量在18 mJ以上，峰值功率高于2.3 MW，在较宽调谐范围内保持了较高的输出能量，输出能量在5 mJ以上的波段占比为78.3%。上述工作为短波红外波段应用提供了一种便捷有效的相干光源。

关键词 非线性光学；光学参量振荡器；短波红外波段；磷酸氧钛钾；角度调谐

中图分类号 O437 **文献标志码** A **DOI**: 10.3788/CJL230599

1 引 言

波长为2～3 μm的红外光处于近红外(一般指0.78～2.50 μm)与中红外(2.5～25.0 μm)的过渡区域，该波段也被称为短波红外波段。红外光在与多种气体分子和生物组织等的相互作用中表现出独特的性质，因此在温室气体和工业气体监测[1-4]、微生物检测[5]以及医疗诊断[6]等领域中有着广泛的应用。该波段的相干光源在应用中发挥着重要的作用，这些光源主要分为两类：掺Tm^{3+}、Ho^{3+}或Er^{3+}等稀土离子的固体或光纤激光器[7-10]及基于非线性频率变换的光学参量振荡器(OPO)[11-14]。一些应用领域(例如多成分分子光谱分析)对光源的调谐性能提出了较高要求。成熟的商用激光器和非线性晶体使OPO成为一种便捷的相干光源，可根据需求设计参数，实现指定波长范围的不间断调谐输出。波长为1.06 μm的Nd:YAG激光器泵浦的磷酸氧钛钾(KTP)[11]、砷酸氧钛钾[12]、周期极化铌酸锂[13]以及周期结构KTP[14]等晶体常被用于短波红外波段的OPO。

在众多非线性晶体中，块状KTP因其光学和力学性能[15-16]而成为一种综合性能优良的OPO介质。较大的非线性系数利于降低OPO起振阈值，实现高效的能量转换；多样的相位匹配形式和较宽的匹配波段有助于获得较大的波长调谐范围(特别是角度调谐)；较高的光损伤阈值保证其可在高功率/能量下运转；较低的成本和成熟的生长加工工艺使其得到广泛应用。研究者们利用KTP晶体对2 μm以上波段(商用激光器不易覆盖)的OPO开展了大量的工作，一些OPO光源已被用作长波红外OPO[17]和差频[18]的泵浦源。以往的大部分研究集中在2.1 μm简并点附近[11,17-21]，高重复频率内腔运转的近简并OPO的输出平均功率先后达到了46 W[19]和70 W[20]。相比之下，2.4 μm以上波段光源的报道较少。2010年，彭跃峰等[22]利用Nd:YAG激光器泵浦反转双KTP晶体内腔OPO，实现了2.68 μm相干光输出。2012年，Bai等[23]利用端面泵浦Nd:YAG内腔结构，实现了1.81 μm和2.58 μm双波长输出。2017年，卞进田[24]利用反转双KTP晶体实现了2.49～2.73 μm调谐输出。2019年，李浩宁等[25]利用单KTP晶体平行平面腔OPO实现了2.4～2.8 μm调谐输出，最高脉冲能量为12.6 mJ。

传统的波段划分方法将2.5 μm作为近红外与中红外的界限，导致了以2.5 μm为中心的相干光源的发展相对薄弱。对于多种化学和生物成分，2～3 μm波段内的光谱信息最丰富，因此该波段的宽调谐光源的研发具有重要意义。本文研究了高能量ns脉冲泵浦KTP晶体OPO，在较小晶体转角下实现了2.05～2.97 μm

收稿日期：2023-03-09；**修回日期**：2023-04-06；**录用日期**：2023-04-28；**网络首发日期**：2023-05-08

基金项目：中国科学院青年创新促进会(2019204)、雄安新区科技创新专项任务(2022XAGG0181)、辽宁省"兴辽英才"计划(XLYC200774)

通信作者：*qifeng@sia.cn

宽调谐输出。比较了单程泵浦的透射式 OPO（SP-OPO）和双程泵浦的反射式 OPO（DP-OPO）两种结构，后者具有更低的起振阈值和更好的调谐平坦性。

2 实验设计

波长为 1.06 μm 的激光泵浦 KTP 晶体 OPO 的一种常用相位匹配形式（II 类匹配，x-z 主平面 θ 角调谐）如图 1 所示。根据文献[26]给出的色散方程，计算出的不同晶体角度（内角）下产生的寻常光（y 主轴偏振）与非寻常光（x-z 面内偏振）波长分别如图 1 中实线和虚线所示。$\theta>50°$（区域 1）的非寻常光和 $\theta<50°$（区域 2）的寻常光波长都可以覆盖 2～3 μm。以往的报道[22-25]更多使用 $\theta>50°$ 的晶体切割方式，其有效非线性系数较大。另一方面，对于相同的调谐范围，区域 1 所需的晶体旋转角度更大，晶体的尺寸限制了上述报道的调谐宽度。在区域 2 内，寻常光波长随匹配角变化的斜率更大，即较小的转角覆盖较宽的波段。理论上，利用 $\theta\approx48°$ 时切割的 KTP 晶体结合适当镀膜的腔镜，通过 ±4°（外角）的旋转可以实现 2.2～3.0 μm 调谐。图 1 中的非寻常光作为信号光谐振，寻常光作为闲频光输出。

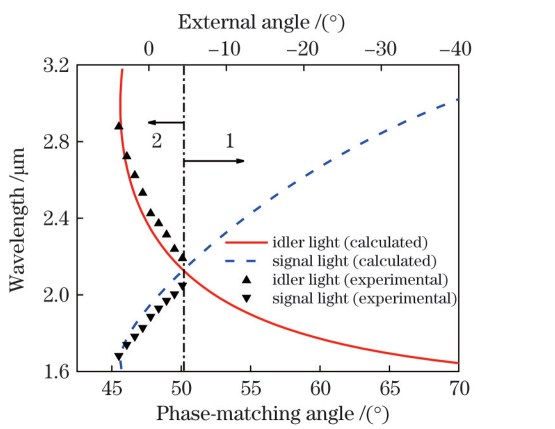

图 1 波长为 1.06 μm 的激光泵浦 KTP 晶体 OPO 的 II 类相位匹配调谐曲线

Fig. 1 Type-II phase-matching tuning curves of 1.06 μm laser pumping KTP-OPO

在此设计基础上构建的实验装置如图 2 所示。Nd：YAG 调 Q 激光器输出的波长为 1.06 μm、脉冲宽度为 7.8 ns、重复频率为 10 Hz、光束直径为 8 mm 的激光作为 OPO 泵浦光。泵浦光先经过由半波片（HWP）和布儒斯特偏振片（BP）组成的可调衰减组件，再经过隔离器（ISO），进入平行平面 OPO 腔。实验中采用了两种 OPO 结构。图 2（a）为单程泵浦的透射式 SP-OPO，其腔镜 M3 和 M4 相同（CaF_2 基底，对 1.65～2.00 μm 信号光高反，对 1.06 μm 泵浦光和 2.2～3.0 μm 闲频光高透），腔长为 28 mm。KTP 晶体尺寸为 10 mm×8 mm×20 mm，切角为 $\theta=47.8°$、$\varphi=0°$，通光面镀 1.06 μm 和 1.65～3.00 μm 增透膜。使用两个长波通滤光片（LP）（CaF_2 基底，对 1.06 μm 高反，对 1.65～3.00 μm 高透）分离输出的闲频光与剩余的泵浦光。图 2（b）为双程泵浦的反射式 DP-OPO，腔镜 M4 被替换为 M4′，将泵浦光、信号光和闲频光全部反射。闲频光透过 M2（CaF_2 基底）和长波通滤光片 LP，利用脉冲能量计对其进行测量。

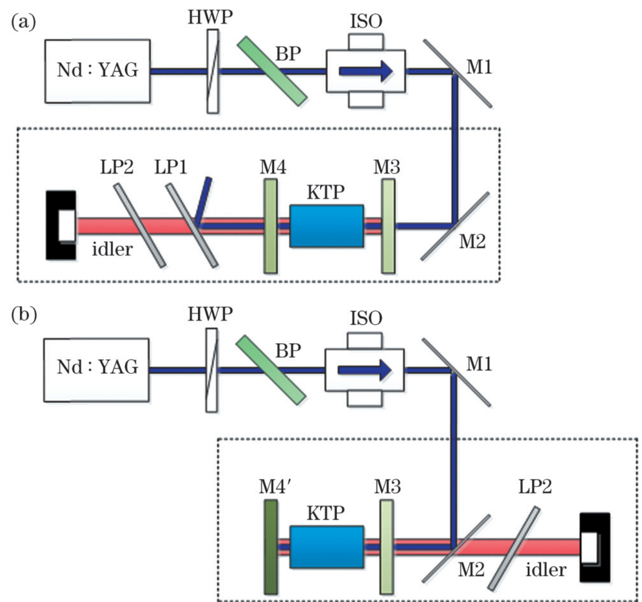

图 2 波长为 1.06 μm 的激光泵浦 KTP 晶体 OPO 的实验装置示意图。（a）SP-OPO；（b）DP-OPO

Fig. 2 Schematics of experimental devices of 1.06 μm laser pumping KTP-OPO. (a) SP-OPO; (b) DP-OPO

3 实验结果分析

使用光谱仪测量 OPO 的输出波长。如图 3 所示，KTP 晶体 OPO 在正入射时的输出波长为 2.43 μm（主峰），1.89 μm 处的次峰对应信号光波长。旋转晶体记录图 1 中散点的波长值，变化趋势与计算曲线基本相符。使用热释电光束质量分析仪观察其输出光斑，如图 3 中插图所示。

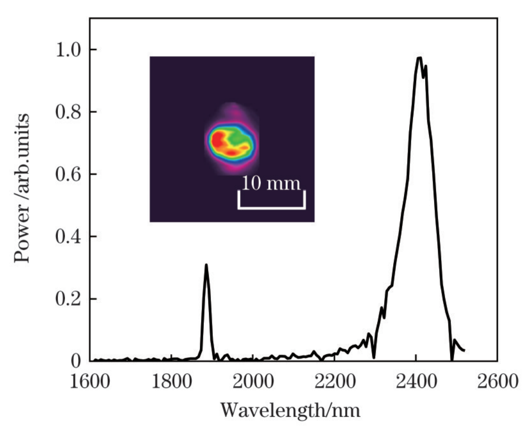

图 3 正入射时 KTP 晶体 OPO 的输出光谱（插图为 OPO 的输出光斑）

Fig. 3 Output spectrum of KTP-OPO at normal incidence with output beam profile of OPO shown in inset

通过调整半波片改变泵浦光能量，测量 2.43 μm 处两种 OPO 结构的输入输出关系，结果如图 4 所示。SP-OPO 的阈值高达 209.3 mJ，DP-OPO 的阈值(70.46 mJ)显著降低。当输出脉冲能量达到(略高于)18 mJ 时，SP-OPO 与 DP-OPO 分别需要 328 mJ 和 148.3 mJ 的泵浦能量，相应的斜率效率分别为 24.9% 和 27.9%，光-光转换效率分别为 5.62% 和 12.38%。

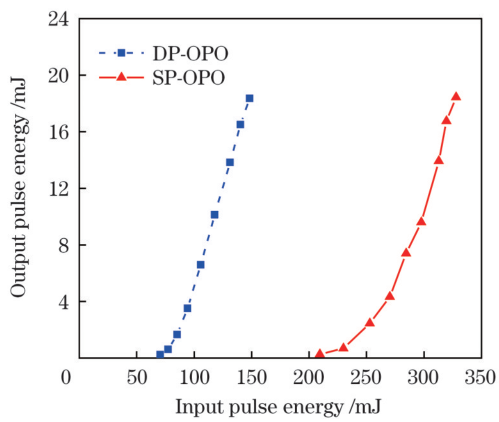

图 4　波长为 2.43 μm 时 SP-OPO 和 DP-OPO 的输入输出特性

Fig. 4　Input-output characteristics of SP-OPO and DP-OPO when wavelength is 2.43 μm

如文献[27]所述，泵浦反射双程增益能够降低 OPO 的阈值，提高转换效率并缩短起振时间。利用长波长型铟镓砷光电二极管(上限波长为 2.6 μm，带宽为 25 MHz)观察的输入和输出脉冲分别如图 5 中虚线和实线所示。以激光器 Q 开关时钟为触发信号，保证输入与输出脉冲的时序一致。DP-OPO 和 SP-OPO 输出脉冲的二极管响应宽度分别为 13.6 ns 和 14.0 ns，小于泵浦脉冲宽度 19.6 ns。与 SP-OPO[图 5(b)]相比，DP-OPO[图 5(a)]的闲频光脉冲形成更早。由于泵浦反射结构的增益高、阈值低，信号光/闲频光脉冲很快形成，其峰值的出现早于泵浦光脉冲。类似的现象在内腔 OPO 实验中已有报道[28]，本文的泵浦反射结构与内腔结构有相似之处。目前，商用的长波长型铟镓砷二极管的响应带宽普遍较小(不超过 50 MHz)，暂时无法直接采集 ns 宽度的脉冲，上述测量的脉宽值大于真实值。利用硅二极管(带宽为 400 MHz)测量得到泵浦光的脉冲宽度为 7.8 ns，OPO 的输出脉冲宽度应小于 7.8 ns，估计对应的峰值功率超过 2.3 MW。

在一定的泵浦能量下，通过旋转 KTP 晶体测量 OPO 输出能量随波长的变化。如图 6 所示，保持两种结构在正入射时的输出近似相等(略大于 18 mJ)，SP-OPO 和 DP-OPO 输入的泵浦能量分别为 148.3 mJ 和 328 mJ。当晶体(外角)从 −6°旋转到 4.6°，输出波长从 2.05 μm 变化至 2.97 μm。受腔镜镀膜工艺的影响，M3 的实际透射率从 2.0 μm 处的低于 1% 逐渐增加到 2.2 μm 处的高于 98%，当闲频光波长小于 2.2 μm 时，对应的信号光波长大于 2.06 μm，腔镜对其也有一定的

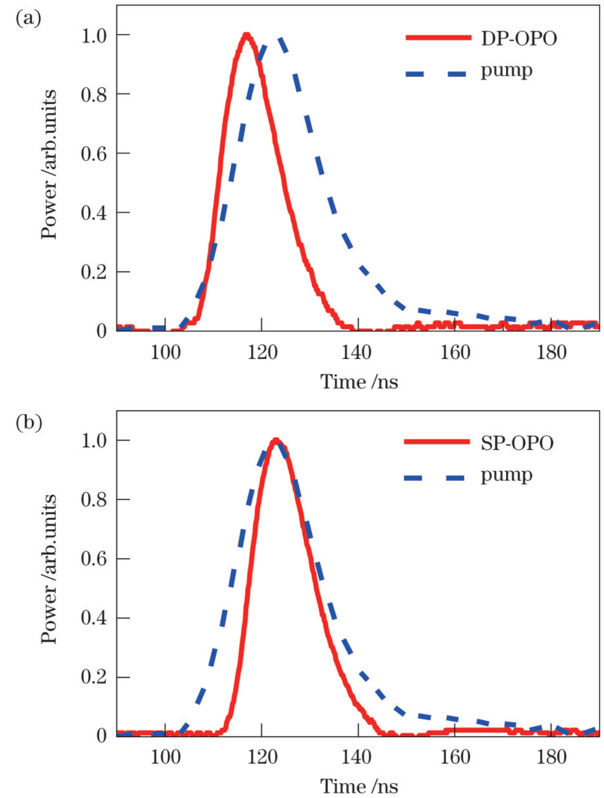

图 5　DP-OPO 和 SP-OPO 的输入和输出脉冲包络。(a)DP-OPO；(b)SP-OPO

Fig. 5　Pulse envelopes of input and output in DP-OPO and SP-OPO. (a) DP-OPO; (b) SP-OPO

透射率。因此，在 2.2 μm 以下的区域，测得的输出能量也包含了部分信号光能量。利用格兰棱镜的偏振分束作用，排除了信号光的能量，保证 OPO 输出纯净的单色光。

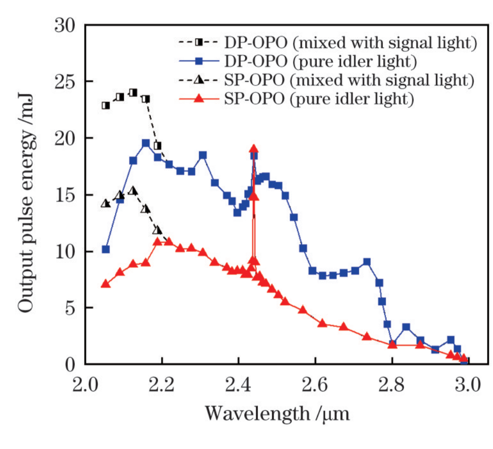

图 6　SP-OPO 和 DP-OPO 波长调谐过程中的输出脉冲能量变化

Fig. 6　Changes of output pulse energy during SP-OPO and DP-OPO wavelength tuning processes

图 6 表明，随着波长的增加，OPO 输出总体呈下降趋势。形成这一趋势的原因有两点：第一，闲频光的波长增大，其与信号光的频率乘积 $\omega_i\omega_s$ 减小，其中，ω_i 为闲频光的频率，ω_s 为信号光的频率；第二，长波长对应的相位匹配角更小，有效非线性系数 $d_{eff}=d_{24}\sin\theta$ 更

小，其中，d_{24}为KTP晶体的二阶非线性张量元。由于OPO阈值(P_{th})反比于$d_{eff}^2\omega_i\omega_s$，在上述两因素的叠加作用下，随着输出波长的增加，阈值升高，因此输入泵浦功率(P_{in})与阈值的比值$N=P_{in}/P_{th}$减小，参量增益和转换效率降低[29]。如图6所示，晶体倾斜引起的菲涅耳反射损耗导致SP-OPO输出急剧下降(正入射位置处有明显的尖峰)。受晶体宽带增透膜工艺的影响，2 μm以上波段的实际反射率接近3%(远不及1.06 μm单波长的0.13%水平)，几何偏折损耗引起阈值升高、输出降低。相比之下，DP-OPO的输出曲线整体高于SP-OPO。在148.3 mJ的泵浦能量下，波长2.05~2.57 μm范围内的输出能量超过了10 mJ，覆盖了总调谐范围的56.5%；输出能量大于5 mJ的波长延伸至2.77 μm，覆盖了总调谐范围的78.3%。根据激光器光束直径8 mm和脉冲宽度7.8 ns可知，当前的泵浦强度约为38 MW·cm^{-2}。即使考虑正向和反向泵浦光强叠加，其2倍也远低于KTP晶体的损伤阈值(约为2 GW·cm^{-2})[30]。因此，该OPO光源的输出水平还有进一步提升的空间。

4 结 论

利用商用Nd:YAG脉冲激光器泵浦KTP晶体OPO，实现了波长为2.05~2.97 μm的短波红外相干光输出。采用了与以往报道不同的相位匹配调谐区域，在较小的晶体转角下，获得了较宽的调谐范围。比较了单程与双程泵浦的两种OPO结构，验证了双程泵浦OPO的优越性：更低的阈值和更高的输出效率等。其最高输出脉冲能量在18 mJ以上，脉冲宽度小于7.8 ns，峰值功率高于2.3 MW，在较宽调谐范围内保持较高的输出能量，输出能量在5 mJ以上的波段占比78.3%。该光源覆盖了以2.5 μm为中心的近红外与中红外过渡波段，便捷的大范围角度调谐可用于光谱分析，较高的峰值功率使DP-OPO可作为半导体晶体长波红外光源的泵浦源。

参 考 文 献

[1] Barria J B, Mammez D, Cadiou E, et al. Multispecies high-energy emitter for CO_2, CH_4, and H_2O monitoring in the 2 μm range[J]. Optics Letters, 2014, 39(23): 6719-6722.

[2] 尹旭坤, 董磊, 武红鹏, 等. 面向SF_6气体绝缘设备故障检测的光声CO气体传感器设计和优化[J]. 物理学报, 2021, 70(17): 170701.
Yin X K, Dong L, Wu H P, et al. Design and optimization of photoacoustic CO gas sensor for fault diagnosis of SF_6 gas insulated equipment[J]. Acta Physica Sinica, 2021, 70(17): 170701.

[3] Raza M, Ma L H, Yao S C, et al. High-temperature dual-species (CO/NH_3) detection using calibration-free scanned-wavelength-modulation spectroscopy at 2.3 μm[J]. Fuel, 2021, 305: 121591.

[4] 姜寿林, 靳伟, 陈非凡, 等. 基于空芯光纤光热光谱技术的高灵敏度CO_2检测[J]. 光学学报, 2021, 41(13): 1306004.
Jiang S L, Jin W, Chen F F, et al. Carbon dioxide detection with high sensitivity based on photo-thermal spectroscopy in hollow-core optical fiber[J]. Acta Optica Sinica, 2021, 41(13): 1306004.

[5] 田燕龙, 王毅, 王箫, 等. 近红外光谱技术在微生物检测中的应用进展[J]. 光谱学与光谱分析, 2022, 42(1): 9-14.
Tian Y L, Wang Y, Wang X, et al. Advances in detection of microorganisms using near-infrared spectroscopy[J]. Spectroscopy and Spectral Analysis, 2022, 42(1): 9-14.

[6] Degirmenci T, Gunlusoy B, Kozacioglu Z, et al. Comparison of Ho: YAG laser and pneumatic lithotripsy in the treatment of impacted ureteral stones: an analysis of risk factors[J]. The Kaohsiung Journal of Medical Sciences, 2014, 30(3): 153-158.

[7] Zhu G W, Zhu X S, Balakrishnan K, et al. Fe^{2+}: ZnSe and graphene Q-switched singly Ho^{3+}-doped ZBLAN fiber lasers at 3 μm[J]. Optical Materials Express, 2013, 3(9): 1365-1377.

[8] Guo L L, Wang M R, Zhang Y F, et al. Mid-infrared dual-wavelength passively Q-switched Er: SrF_2 laser by $CsPbCl_3$ quantum dots absorber[J]. Crystals, 2022, 12(9): 1265.

[9] 闵欢欢, 刘广华, 翟学君, 等. 单掺钬固体激光器的研究进展[J]. 激光与光电子学进展, 2022, 59(21): 2100002.
Min H H, Liu G H, Zhai X J, et al. Research progress of holmium-doped solid-state lasers[J]. Laser & Optoelectronics Progress, 2022, 59(21): 2100002.

[10] 樊浩泽, 梁金辉, 郑树锴, 等. 2.8 μm中红外同步泵浦锁模光纤激光器[J]. 中国激光, 2022, 49(1): 0101020.
Fan H Z, Liang J H, Zheng S K, et al. 2.8 μm mid-infrared synchronously pumped mode-locked fiber laser[J]. Chinese Journal of Lasers, 2022, 49(1): 0101020.

[11] Lin J T, Montgomery J L. Generation of tunable mid-IR (1.8-2.4 μm) laser from optical parametric oscillation in KTP[J]. Optics Communications, 1990, 75(3/4): 315-320.

[12] 朱雅琛, 兰戈, 李彤, 等. 脉冲式2 μm $KTiOAsO_4$光参变振荡器[J]. 光学学报, 2007, 27(11): 2059-2063.
Zhu Y C, Lan G, Li T, et al. 2 μm $KTiOAsO_4$ optical parametric oscillator[J]. Acta Optica Sinica, 2007, 27(11): 2059-2063.

[13] Wang S T, Tulake Y, Sulaiman D, et al. Tunable 2.3 - 3 μm optical vortex parametric laser[J]. Laser Physics, 2022, 32(4): 045001.

[14] Edwards T J, Turnbull G A, Dunn M, et al. Continuous-wave, singly-resonant, optical parametric oscillator based on periodically poled $KTiOPO_4$[J]. Optics Express, 2000, 6(3): 58-63.

[15] Zumsteg F C, Bierlein J D, Gier T E. $K_xRb_{1-x}TiOPO_4$: a new nonlinear optical material[J]. Journal of Applied Physics, 1976, 47(11): 4980-4985.

[16] Bierlein J D, Vanherzeele H. Potassium titanyl phosphate: properties and new applications[J]. Journal of the Optical Society of America B, 1989, 6(4): 622-633.

[17] Miyamoto K, Ito H. Wavelength-agile mid-infrared (5-10 μm) generation using a galvano-controlled $KTiOPO_4$ optical parametric oscillator[J]. Optics Letters, 2007, 32(3): 274-276.

[18] Yan D X, Xu D G, Wang Y Y, et al. High-repetition-rate, tunable and coherent mid-infrared source based on difference frequency generation from a dual-wavelength 2 μm laser and GaSe crystal[J]. Laser Physics, 2018, 28(12): 126205.

[19] 彭跃峰, 谢刚, 王卫民, 等. 46 W腔内光参量振荡高重复频率2 μm激光器[J]. 中国激光, 2009, 36(1): 33-36.
Peng Y F, Xie G, Wang W M, et al. Intracavity optical parametric oscillator high-repetition-rate 2 μm laser with 46 W output power[J]. Chinese Journal of Lasers, 2009, 36(1): 33-36.

[20] Cui Q J, Shu X W, Le X Y, et al. 70-W average-power doubly resonant optical parametric oscillator at 2 μm with single KTP[J]. Applied Physics B, 2014, 117(2): 639-643.

[21] 谢小兵, 李世光, 朱小磊, 等. 2.05 μm单谐振纳秒脉冲光参量振荡器特性研究[J]. 中国激光, 2016, 43(12): 1208002.
Xie X B, Li S G, Zhu X L, et al. Characteristics of single resonant nanosecond pulse optical parametric oscillator with output wavelength of 2.05 μm[J]. Chinese Journal of Lasers, 2016, 43(12): 1208002.

[22] 彭跃峰, 魏星斌, 王卫民, 等. 近衍射极限腔内光参量振荡2.7 μm

激光器[J]. 中国激光, 2010, 37(9): 2376-2379.
Peng Y F, Wei X B, Wang W M, et al. Intracavity optical parametric oscillator 2.7 μm laser with near diffraction limit beam quality[J]. Chinese Journal of Lasers, 2010, 37(9): 2376-2379.
[23] Bai F, Wang Q P, Liu Z J, et al. 1.8 μm optical parametric oscillator based on $KTiOPO_4$[J]. Laser Physics, 2012, 22(12): 1797-1802.
[24] 卞进田. KTP OPO 产生 2.7 μm 波段高峰值功率激光实验研究[J]. 光电技术应用, 2017, 32(4): 22-25.
Bian J T. Experimental research on 2.7 μm wave band laser with high peak power generated by KTP optical parametric oscillator[J]. Electro-Optic Technology Application, 2017, 32(4): 22-25.
[25] 李浩宁, 张大成, 朱江峰, 等. 纳秒中红外可调谐参量激光研究[J]. 光学学报, 2019, 39(11): 1114002.
Li H N, Zhang D C, Zhu J F, et al. Nanosecond mid-infrared tunable parametric laser[J]. Acta Optica Sinica, 2019, 39(11): 1114002.
[26] Kato K, Takaoka E. Sellmeier and thermo-optic dispersion formulas for KTP[J]. Applied Optics, 2002, 41(24): 5040-5044.
[27] Bjorkholm J, Ashkin A, Smith R. Improvement of optical parametric oscillators by nonresonant pump reflection[J]. IEEE Journal of Quantum Electronics, 1970, 6(12): 797-799.
[28] Yan D X, Wang Y Y, Xu D G, et al. High power, widely tunable dual-wavelength 2 μm laser based on intracavity KTP optical parametric oscillator[J]. Journal of Physics D: Applied Physics, 2017, 50(3): 035104.
[29] Sutherland R L. Handbook of nonlinear optics[M]. 2nd ed. New York: Marcel Dekker, 2003: 144-145.
[30] Ahmed F. Laser damage threshold of $KTiOPO_4$[J]. Applied Optics, 1989, 28(1): 119-122.

Widely Tunable and High Pulse Energy Short-Wave Infrared Optical Parametric Oscillator

Liu Pengxiang[1,2,3,4], Li Wei[1,2,3], Qi Feng[2,3*], Niu Chuncao[1,2,3], Li Weifan[2,3], Fu Qiaoqiao[2,3,4], Guo Liyuan[2,3], Li Zhongyang[5]

[1]*College of Information Engineering, Shenyang University of Chemical Technology, Shenyang* 110142, *Liaoning, China*;
[2]*Shenyang Institute of Automation, Chinese Academy of Sciences, Shenyang* 110169, *Liaoning, China*;
[3]*Key Laboratory of Liaoning Province in Terahertz Imaging and Sensing, Shenyang* 110169, *Liaoning, China*;
[4]*University of Chinese Academy of Sciences, Beijing* 100049, *China*;
[5]*College of Electric Power, North China University of Water Resources and Electric Power, Zhengzhou* 450045, *Henan, China*

Abstract

Objective The 2–3 μm short-wave infrared band exhibits unique properties during interactions with gas molecules and biological tissues. Thus, it finds applications in various domains such as remote sensing of greenhouse gases, atmospheric pollution, and medical treatments. Coherent sources in this band play a key role in the above fields and the tunability of the coherent sources is an important factor, especially in multiple molecule spectroscopy. OPOs have proved to be effective light sources with desired wavelengths, owing to the following merits: the commercial availability of well-developed lasers and nonlinear crystals, coupled with their agile frequency tunability. Bulk $KTiOPO_4$ (KTP) serves as an excellent OPO medium owing to its high optical damage threshold, moderate nonlinearity, wide phase-matching (PM) wavelength region, and low cost. However, most previous studies focused on doubly resonant operation at wavelengths below 2.4 μm. In this study, we perform an experimental analysis of nearly singly resonant KTP-OPO with a wide tuning range of 2.05–2.97 μm under a small rotation angle.

Methods A commonly used PM geometry of Nd∶YAG laser pumping KTP-OPO (type-II, θ-tuning in the x-z plane) is presented in Fig. 1. In the range of $\theta<50°$, the output wavelength changes rapidly with the PM angle. Thus, a KTP cut at $\theta\approx48°$ incorporating properly coated cavity mirrors can theoretically perform a singly resonant OPO, covering 2.2–3.0 μm under a rotation (external) angle of $\pm4°$. The experimental setup of the OPO is illustrated in Fig. 2. A Q-switched Nd∶YAG laser is used as the pump source. The pump pulses pass through a variable attenuator (comprising a half-wave plate and a Brewster polarizer) and an isolator (ISO) and are incident on a plane-parallel OPO cavity. Two configurations are tested: single-pass OPO (SP-OPO) and double-pass OPO (DP-OPO). In the first case, the cavity mirrors M3 and M4 are identical (CaF_2 coated with high-reflection films at 1.65–2.00 μm and anti-reflection films at 1.06 μm and 2.2–3.0 μm) with a spacing of 28 mm. Two long-pass filters (CaF_2 coated with high-reflection films at 1.06 μm and anti-reflection films at 1.65–3.00 μm) are used to block the residual pump. In the second case, M4 is changed into a total reflection mirror M4′ at 1.06 μm and 1.65–3.00 μm. The backward idler beam is transmitted through M2 (CaF_2) and a long-pass filter and is detected by a pyroelectric sensor. The KTP crystal has cut angles of $\theta=47.8°$ and $\varphi=0°$, and dimensions of 10 mm×8 mm×20 mm, and is mounted on a rotation stage.

Results and Discussions The output wavelength of the KTP-OPO at normal incidence is measured by a spectrometer. In Fig. 3, the main peak at 2.43 μm is corresponding to the idler light, and the secondary peak at 1.89 μm is corresponding to the resonant signal light. The values at different KTP incidence angles, plotted as scatters in Fig. 1, almost follow the calculated curves. By adjusting the half wavelength plate and changing the pump attenuation, the relationship between the OPO output and pump input is observed at

2.43 μm (Fig. 4). The SP-OPO has an extremely high threshold of 209.3 mJ, which is approximately 3 times that (70.46 mJ) of the DP-OPO. The idler pulse energies of SP- and DP-OPO rise above 18 mJ under pump energies of 328 mJ and 148.3 mJ with slope efficiencies of 24.9% and 27.9%, respectively. The input and output pulse envelopes are captured with an InGaAs photodiode. Figure 5 shows that the idler pulse of DP-OPO arises earlier than that of SP-OPO. The tuning curves are measured under given pump energies. Here, the outputs of the two configurations are set to be approximately equal at normal incidence. The wavelength band extends from 2.05 μm to 2.97 μm (Fig. 6) by rotating the PM angle of KTP from −6° to 4.6°. In the region below 2.2 μm, both the idler and signal lights are emitted from the OPO cavities because the transmittance of M3/M4 increases gradually from less than 1% at 2.0 μm to more than 98% at 2.2 μm. The signal energies are excluded by separating the two orthogonally polarized wavelengths with a Glan prism. The curve of DP-OPO is mostly higher than that of SP-OPO. Under a pump energy of 148.3 mJ, the output at 2.05–2.57 μm exceeds 10 mJ (56.5% coverage), and that at 2.77 μm exceeds 5 mJ (78.3% coverage).

Conclusions We present a tunable short-wave infrared source based on a Nd: YAG laser pumping KTP-OPO. A wide tuning range from 2.05 μm to 2.97 μm is obtained under a small KTP crystal rotation angle. The highest output energy exceeds 18 mJ. The advantages of the pump-reflected double-pass OPO over the single-pass OPO are demonstrated, including the reduced threshold, enhanced efficiency, and decreased build-up time. The wavelength coverage with an output above 5 mJ is 78.3%. The continuous and wide tunability, as well as the high peak power, can find application in the fields such as multiple gas analysis and DP-OPO can be used as the pump source of semiconductor crystal based nonlinear long-wave generation.

Key words nonlinear optics; optical parametric oscillator; short-wave infrared band; potassium titanyl phosphate; angle tuning